lajss.org©
Latin American Journal of Solids and Structures
www.lajss.org

A Novel Multilayer 3D Hexahedral Finite Element for Static and Free Vibration Analysis of Isotropic and Functionally Graded Structures

Randa Bourenane[a*] [ORCID: 0009-0006-5416-8425], Belkacem Amieur [b], Sifeddine Abderrahmani [a], Abdulrahman M. AL-Nadhari [c]

[a] Department of Civil Engineering, Laboratory of Applied Civil Engineering (LGCA), University of Echahid Cheikh Larbi Tebessi, Tebessa, Algeria. Email: sifeddine.abderrahmani@univ-tebessa.dz

[b] Reliability of Materials and Structures Laboratory, TAHRI Mohamed University of Bechar, Algeria. Email: amieur.belkacem@univ-bechar.dz

[c] LARGHYDE Laboratory, Department of Civil Engineering and Hydraulics, Faculty of Sciences and Technology, University of Biskra, BP 145 RP, 07000, Biskra, Algeria. Email: a.alnadhari@univ-biskra.dz

* Corresponding author, E-mail address: randa.bourenane@univ-tebessa.dz

Abstract

This work presents, for the first time, a high-order three-dimensional quadrature element formulation for the hybrid membrane and bending analysis of plate and beam structures under static and free vibration conditions. The proposed element represents a novel contribution to the field of computational mechanics, combining high-order polynomial interpolation with advanced quadrature numerical integration to accurately capture the full 3D stress and displacement fields within beam and plate elements. Unlike traditional 2D formulations, this new approach accounts for through-thickness deformation and stress variation, offering enhanced modeling capabilities for both thin and thick beams and plates. Separate yet consistent formulations are developed for in-plane (membrane) and out-of-plane (bending) behaviors, and their coupling is naturally integrated into the 3D framework. The use of extensive numerical examples demonstrates the accuracy, efficiency, and robustness of the proposed element, especially in representing complex boundary conditions, and higher vibration modes for isotropic and functionally graded (FG) material case. The obtained results show rapid convergence, close agreement with analytical and benchmark solutions, and accurate prediction of natural frequencies across different boundary conditions and structural configurations. This pioneering work opens new perspectives for high-fidelity structural modeling using three-dimensional high-order quadrature finite elements.

Keywords

High-order finite element; 3D plate analysis; Free vibration; multilayer Hexahedral formulation; Numerical integration; Functionally graded materials (FGMs)

List of Symbols

x, y, z : Cartesian coordinates
ξ, η, ζ : Natural (isoparametric) coordinates
$a = L, b, h$: Element dimensions (length, width, thickness)
U, V, W : Displacements along x, y, z directions, respectively
$\{u\}$: Global nodal displacement vector
$\{u_e\}$: Element displacement vector
$\{a\}$: Vector of unknown coefficients
$[N]$: Shape function matrix
$[P]$: Displacement interpolation matrix
$[Q]$: Strain interpolation matrix

$[A]$: Transformation matrix
$[B]$: Strain displacement matrix
$\{\varepsilon\}$: Strain vector
$\gamma_{xy}\gamma_{yz}\gamma_{zx}$: Shear strains
$[D]$: Elasticity (constitutive) matrix
E : Young's modulus
ν *: Poisson's ratio*
ρ *: Material density*
D: Bending rigidity
$[K_{\mathrm{e}}]$: Element stiffness matrix
$[M_{\mathrm{e}}]$: Element mass matrix
$[K]$: Global stiffness matrix
$[M]$: Global mass matrix
$\{F\}$: Global nodal force vector
P: Concentrated load
q, q_o: Distributed transverse load
ω: Natural frequency
W: Dimensionless deflection
λ: Non-dimensional frequency parameter
ϖ: Non-dimensional frequency parameter (FGM plates)
EI : Bending stiffness of beam section
n: Power-law exponent (FGM index)
V_c: Ceramic volume fraction
E_c, E_m: Young's modulus of ceramic and metal
ρ_c, ρ_m: Density of ceramic and metal
ν_c, ν_m: Poisson's ratios of ceramic and metal

Abbreviations
FEM: Finite Element Method
MLH8N: Multi-Layer Hexahedral 8-Node
FGM: Functionally Graded Material
DOF: Degree of Freedom
CF: Clamped–Free
CC: Clamped–Clamped
SS: Simply Supported
SSSS: Fully Simply Supported
CCCC: Fully Clamped
CFFF: Clamped–Free–Free–Free
CCFF: Clamped–Clamped–Free–Free
CSSF: Clamped–Simply Supported–Simply Supported–Free
SSSF: Simply Supported–Simply Supported–Simply Supported–Free
SFSF: Simply Supported–Free–Simply Supported–Free
CCCF: Clamped–Clamped–Clamped–Free
CFCF: Clamped–Free–Clamped–Free
CFSF: Clamped–Free–Simply Supported–Free
Abbreviation S, C and F stand for simply supported, clamped and free edges respectively

1 INTRODUCTION

The precise representation and examination of beam and plate structures have historically been fundamental to computational mechanics, owing to their widespread utilization in civil, mechanical, aerospace, and marine engineering disciplines, as highlighted by Lamraoui et al. (2024). These structural elements play crucial roles in bridges, aircraft fuselages, ship hulls, and industrial machinery, where they are subjected to complex loading scenarios involving both in-plane (membrane) and out-of-plane (bending) forces, as highlighted by Słota and Wosatko (2025). Capturing these interactions with high precision is essential to ensure structural integrity, optimal performance, and safety.

Nevertheless, conventional finite element approaches for the analysis of plates and membranes reveal extensively recognized constraints, such as the occurrence of shear locking in thick plates, as illustrated by the modified Mindlin formulation, as discussed by Ren et al. (2022); sensitivity to mesh deformation in membrane components incorporating drilling rotations, as shown by Sheng et al. (2025); and challenges in accurately modeling cracked plates, where Ma et al. (2024) validated an analytical wave propagation method that compares favorably against conventional FEM results. While displacement-based elements remain widely used in engineering practice, these limitations highlight the need for specialized formulations tailored to specific structural applications. To address these challenges, advanced strain-based formulations, such as those developed by (Belounar and Guerraiche, 2014; Bouzidi et al., 2019), have been implemented, successfully alleviating locking issues. Simultaneously, advanced numerical methodologies, encompassing the strategies suggested, have been discussed by Tian et al. (2024), have demonstrated superior accuracy, providing robust and reliable solutions for complex structural applications.

Focusing on strain-based formulations, researchers have developed robust 2D elements to effectively model membrane and bending behaviors. Bouzidi et al. (2019) introduced a strain-based quadrilateral membrane element with linear strain variations for static and dynamic analysis, demonstrating high accuracy. Belarbi and Maalem (2005) formulated an improved rectangular finite element for plane linear elasticity, achieving exact solutions through static condensation. Rebiai et al. (2015) proposed a quadrilateral element with in-plane rotation for 2D linear and dynamic analysis, satisfying rigid body modes. Sabir and Sfendji (1995) developed triangular and rectangular strain-based elements for plane elasticity, incorporating linear and constant strain assumptions to improve accuracy in problems where shearing stress dominates deformation. These 2D formulations laid a strong foundation for capturing membrane behavior but were limited in addressing three-dimensional effects, such as transverse shear and through-thickness stresses.

In parallel with the development of improved finite element formulations, several studies have investigated the dynamic behavior of plate and panel structures. In particular, Pany has conducted extensive research on the vibration and wave propagation characteristics of plate-like structures. Finite element analysis of the free vibration of orthogonally supported multi-span curved panels using high-precision triangular elements provided reliable benchmark solutions, as presented by Pany et al. (2001). Subsequently, the nonlinear vibration behavior of cantilever beams was investigated using simplified nonlinear stiffness models, revealing characteristic hardening responses at large vibration amplitudes, as proposed by Pany and Rao (2002). This methodology was later extended to infinitely long curved panels to determine natural frequencies efficiently using beam functions and triangular finite elements, as investigated by Pany and Parthan (2003). More recently, wave propagation in two-dimensional periodic plate structures has been analyzed to determine dynamic characteristics from phase–frequency relationships, as reported by Pany (2022).

The development of 3D strain-based models has significantly expanded the capabilities of plate analysis, particularly for thick structures. Belarbi and Charif (1999) developed an 8-node hexahedral strain-based finite element with three translational degrees of freedom (U, V, W) per node for plate bending analysis. The formulation demonstrates superior numerical efficiency compared to conventional displacement-based models, as validated through comprehensive testing on both thin and thick plate configurations. Guerraiche et al. (2018) developed an eight-node brick finite element with assumed strain functions, demonstrating excellent performance in linear analysis of both thick and thin plate bending problems. Messai et al. (2018) advanced this approach by developing a nine-node strain-based element for static and free vibration analysis of plates, implemented in ABAQUS, demonstrating superior accuracy in both displacement and natural frequency predictions. Belounar and Guerraiche (2014) introduced a strain-based brick element with a centroidal node and static condensation, optimizing computational efficiency for plate bending. Derradji et al. (2021) developed the SBH8 hexahedral element, effectively addressing shear locking in static and dynamic conditions. Hamadi and Maalem (2010) developed the SBP8C strain-based parallelepiped element, employing static condensation to optimize plate bending analyses for both thick and thin configurations, demonstrating superior accuracy and convergence compared to conventional displacement-based formulations. These 3D strain-based elements effectively capture complex deformations, particularly in shear-critical scenarios, while eliminating locking effects across the full range of plate thicknesses, from thin to thick.

High-order numerical techniques, such as the Quadrature Element Method (QEM), have significantly advanced plate analysis by utilizing high-order polynomial interpolation and efficient numerical integration, ensuring rapid convergence and enabling the modeling of complex geometries with fewer elements compared to traditional Finite Element Method (FEM). Cetkin and Orak (2017) demonstrated QEM's high accuracy and efficiency for the free vibration analysis of point-supported rectangular plates, showing strong agreement with other analytical and numerical solutions and highlighting QEM's capability to handle complex boundary conditions. Xing et al. (2022) reviewed analytical solution methods for eigenvalue problems of rectangular plates, emphasizing the applicability and effectiveness of high-order methods like QEM for vibration analysis

In parallel, functionally graded materials (FGMs) have emerged as advanced composites with continuously varying properties across the thickness, typically described by a power-law distribution, offering enhanced structural and thermal performance compared to traditional laminates. Talha and Singh (2010) applied higher-order shear deformation theory to analyze the static and free vibration behavior of FGM plates, showing that lower gradient indices and smaller thickness ratios lead to higher natural frequencies. Kareem et al. (2025) proposed a novel trigonometric-based displacement function, validated through ANSYS simulations, revealing the significant influence of the power-law index and aspect ratio on vibrational response. Furthermore, Belounar et al. (2022) developed a strain-based finite element combining membrane and bending behaviors, which demonstrated excellent accuracy in both static and free vibration analyses. These studies collectively underline the necessity of advanced modeling strategies to accurately capture the complex mechanical response of FGM structures.

This paper presents the development of a new high-order three-dimensional finite element, the **MLH8N** (**M**ulti-**L**ayer **H**exahedral **8**-**N**ode) for isotropic and FGM composite material, for advanced analysis of plate structures. The proposed element combines polynomial interpolation with a strain-based approach to enable hybrid membrane - bending modeling. With its eight-node configuration and three translational degrees of freedom per node, the MLH8N element effectively addresses common numerical challenges such as locking, accurately models complex boundary conditions, and achieves rapid convergence. Comprehensive validation through analytical and numerical benchmarks demonstrates the superior accuracy and computational efficiency of the element, highlighting its strong potential for optimizing the design and analysis of plate-based structures in various engineering applications.

2 Variational formulation of the MLH8N element

Figure 1 The element is an eight-node hexahedral solid with three degrees of freedom (DOF) per node.

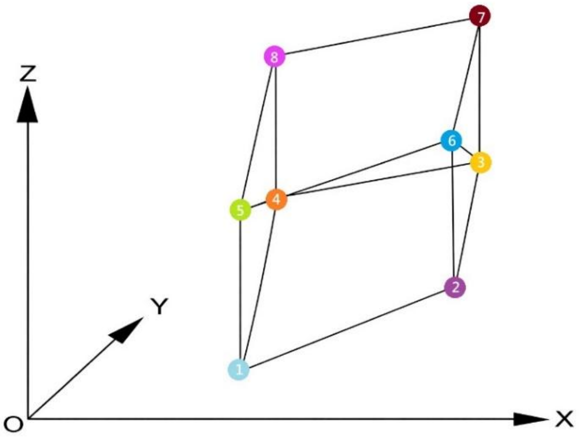

Figure 1 Geometry of the MLH8N element

The final displacement field will be obtained by superposition (Belarbi and Charif, 1999) in order to determine the shape functions ensuring an interpolation between the displacements of the 8-node hexahedral element facilitating the numerical integration by following ξ, η and ζ in the 3 directions.

$$U = a_1 + a_4 y + a_6 z + a_7 x + a_8 \mathrm{xy} + a_9 xz + a_{10} \mathrm{xyz} - a_{12} \frac{y^2}{2} - a_{14} \frac{y^2 z}{2} - a_{16} \frac{z^2}{2} - a_{18} \frac{yz^2}{2} + a_{21} \frac{z}{2} + a_{23} \frac{y}{2} + a_{24} yz$$

$$V = a_2 - a_4 x - a_5 z - a_8 \frac{x^2}{2} - a_{10} \frac{x^2 z}{2} + a_{11} y + a_{12} xy + a_{13} yz + a_{14} xyz - a_{17} \frac{z^2}{2} - a_{18} \frac{xz^2}{2} + a_{19} \frac{z}{2} + a_{20} xz + a_{23} \frac{x}{2} \tag{1}$$

$$W = a_3 + a_5 y - a_6 x - a_9 \frac{x^2}{2} - a_{10} \frac{x^2 y}{2} - a_{13} \frac{y^2}{2} - a_{14} \frac{xy^2}{2} + a_{15} z + a_{16} xz + a_{17} yz + a_{18} xyz + a_{19} \frac{y}{2} + a_{21} \frac{x}{2} + a_{22} xy$$

$$\{U_e\} = \begin{pmatrix} U \\ V \\ W \end{pmatrix} = [P]\{a\} = [N]\{u\} \tag{2}$$

$$\{\varepsilon\} = \begin{pmatrix} \varepsilon_x \\ \varepsilon_y \\ \varepsilon_z \\ \gamma_{xy} \\ \gamma_{yz} \\ \gamma_{zx} \end{pmatrix} = [Q]\{a\} = [B]\{u\} \tag{3}$$

With:

$$\{u\} = \{u_1, v_1, w_1 \ldots \ldots, u_8, v_8, w_8\}^T$$

And $[N]$ is the shape functions obtained from equation (1).

2.1 Automatic evaluation of the matrix [K0]

The evaluation of the elementary stiffness matrix is summarized by the evaluation of the following expression obtained by using the virtual work principle:

$$[k_e] = [A]^{-T}[K_0][A^{-1}] \tag{4}$$

With:

$$[K_0] = \iiint_V [B]^T [D][B] \, dx.dy.dz \tag{5}$$

$$[k_e] = \int_{V^e} [B]^T [D][B] \, dV = [A]^{-T} \left(\int_{V^e} [Q]^T [D][Q] \, dV \right) [A]^{-1} = [A]^{-T} \left(\iiint [Q]^T [D][Q] \, d\xi d\eta d\zeta \right) [A]^{-1} \tag{6}$$

And for the mass matrix is given by:

$$[M_e] = \int_{V^e} \rho [N]^T [N] \, dV = [A]^{-T} \left(\int_{V^e} \rho [P]^T [P] \, dV \right) [A]^{-1} = [A]^{-T} \left(\iiint \rho [P]^T [P] \, d\xi d\eta d\zeta \right) [A]^{-1} \tag{7}$$

Where $[A]$ is the transformation matrix given by:
$[A] = [P_i]_{24\times 24}$ where i is the number of nodes of element used.

$$[A] = \begin{bmatrix} P(0,0,0) \\ P(a,0,0) \\ P(a,b,0) \\ P(0,b,0) \\ P(0,0,h) \\ P(a,0,h) \\ P(a,b,h) \\ P(0,b,h) \end{bmatrix}_{24\times 24} , \begin{Bmatrix} U \\ V \\ W \end{Bmatrix} = [P(x,y,z)]\{a\} \tag{8}$$

Where a, b and h are the element coordinates.
$[B]$ the deformation matrix which links deformations with nodal displacements:

$$[B] = \begin{bmatrix} \varepsilon_{xx=U,x} \\ \varepsilon_{yy=U,y} \\ \varepsilon_{zz=U,z} \\ \gamma_{xy} = U_{,y} + V_{,x} \\ \gamma_{yz} = V_{,z} + W_{,y} \\ \gamma_{xz} = W_{,x} + U_{,z} \end{bmatrix} \tag{9}$$

For the static analysis, the overall equilibrium equation is articulated as follows:

$$[k]\{u\} = \{F\} \tag{10}$$

For the free vibration domain, the global equilibrium equation is expressed as follows:

$$([k] - \omega^2[M])\{u\} = 0 \tag{11}$$

where ω is the natural frequency
And the elasticity matrix [D] for plane stress problems is

$$[D] = D_1 \begin{bmatrix} 1 & v & 0 & 0 & 0 & 0 \\ & 1 & 0 & 0 & 0 & 0 \\ & & D_2 & 0 & 0 & 0 \\ & & & D_3 & 0 & 0 \\ & Symmetrical & & & KD_3 & 0 \\ & & & & & KD_3 \end{bmatrix} \tag{12}$$

$$D_1 = \frac{E}{(1 - v^2)};\ D_2 = \frac{(1 - v)^2}{(1 - 2v)}; D_3 = \frac{(1 - v)}{2} \tag{13}$$

An isoparametric transformation is used to map the natural coordinate system (ξ, η, ζ), defined in the reference domain $-1 \leq \xi, \eta, \zeta \leq 1$, to the physical Cartesian coordinates (x, y, z), where $0 \leq x \leq a$, $0 \leq y \leq b$, and $0 \leq z \leq h$. The mapping is given by:

$$\begin{cases} x = \left(\frac{a}{2}\right)(1 + \xi) \\ y = \left(\frac{b}{2}\right)(1 + \eta) \\ z = \left(\frac{h}{2}\right)(1 + \zeta) \end{cases} \tag{14}$$

For the FGM case, the material properties change thought thickness (Amieur et al., 2017; Amieur et al., 2024; Belounar et al., 2023):

$$\begin{cases} E = (E_c - E_m)V_c + E_m \\ \rho = (\rho_c - \rho_m)V_c + \rho_m \\ v = (v_c - v_m)V_c + v_m \end{cases} \tag{15}$$

Where the volume fraction, according to the power law, is given by:

$$V_c = (\tfrac{z}{h} + \tfrac{1}{2})^n\ ; \quad (n \geq 0) \tag{16}$$

Subscripts c and m refer to ceramic and the metal materials, respectively and n is the volume fraction exponent.

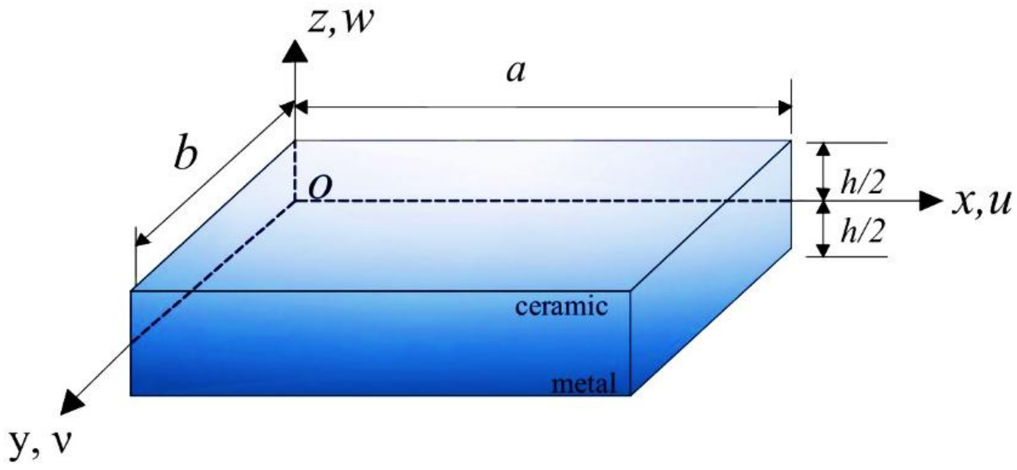

Figure 2 Geometry and coordinate system of functionally graded (FG) plate under consideration

Table 1 Properties of the FGM components

Material	Properties		
	E (N/m²)	Poisson's ratio ν	Density ρ (kg/m³)
Aluminium (Al)	70×10^9	0.30	2707
Alumina (Al_2O_3)	380×10^9	0.30	3800
Zirconia (ZrO_2)	200×10^9	0.30	5700
Stainless steel (SUS304)	207.78×10^9	0.3177	8166
Silicon nitride (Si_3N_4)	322.27×10^9	0.24	2370

3 Linear numerical validation

This section investigates the static and free vibration responses of isotropic and functionally graded (FG) plates using the proposed element. By analyzing various benchmark scenarios with diverse load types and mesh configurations, the accuracy and efficiency of the newly developed formulation are rigorously tested. The resulting numerical data are compared against established analytical solutions and alternative numerical models, demonstrating the robustness and reliability of the current element across a wide range of structural applications.

A summary of the boundary conditions employed in this study is provided in **Table 2.**

Table 2 Types of boundary conditions considered in the present study

Boundary condition	Constrain edges
CCCC	$u = v = w = 0$ at x=0, a and y=0, b
SSSS	$u = w = 0$ at x=0, a and v=w $= 0$ at y=0, b
CFFF	$u = v = w = 0$ at x=0
CCFF	$u = v = w = 0$ at x=0 and y=0
C-F (for beam)	$u = v = w = 0$ at x=0
C-C (for beam)	$u = v = w = 0$ at x=0, a
S-S (for beam)	$u = w = 0$ at x=0, a
CSSF	$u = v = w = 0$ at x=0, v=w $= 0$ at y=0, and $u = w = 0$ at x= a
SSSF	$u = w = 0$ at x=0, a and v=w $= 0$ at y=0
SFSF	$u = w = 0$ at x=0, a
CCCF	$u = v = w = 0$ at x=0, a
CFCF	$u = v = w = 0$ at x=0, a
CFSF	$u = v = w = 0$ at x=0, $u = w = 0$ at x= a

3.1 Static numerical validation

3.1.1 Plane bending of a short cantilever beam

The cantilever beam subjected to shear force is a common evaluation for membrane components. **Figure 3** depicts the mechanical and geometric characteristics of the problem, with displacements calculated at the free end of the beam. The performance of a cantilever beam subjected to a distributed shear force (P=40k) is analyzed as depicted in Figure 3. The examination is performed on membrane elements exhibiting varying degrees of freedom and of rectangular configuration. The analytical solution is delineated in (Timoshenko and Goodier, 1951) as follows:

$$V = \frac{PL^3}{3EI} + \frac{(4+5v)}{2EH}PL = 0.3413 + 0.014 = 0.3553$$

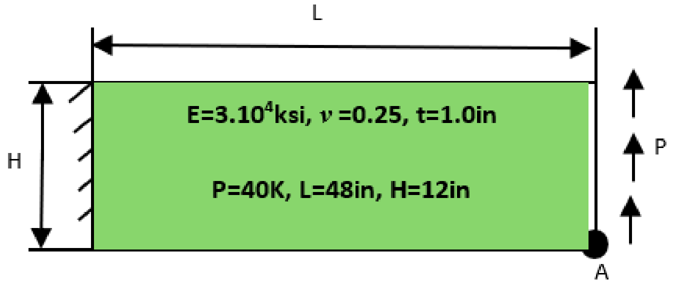

Figure 3 Bending of a short beam under vertical load

The outcomes of the vertical displacements at the conclusion for various mesh densities (M1, M2, and M3) are displayed in **Table 3** below:

Table 3 Vertical deflection at point A

Mesh	Presentation of the study			Analytic solution (Timoshenko and Goodier, 1951)
	Allman (Ibrahimbegović and Frey, 1992)	Frey (Ibrahimbegović and Frey, 1992)	**MLH8N**	
M1 (4x1)	0.3026	0.3283	**0.3283**	**0.3553**
M2 (8x2)	0.3394	0.3460	**0.3461**	
M3 (16x4)	0.3512	0.3529	**0.3533**	

Table 3 presents the vertical displacement at point A for various mesh densities, showing that the developed MLH8N element demonstrates good convergence and competitive accuracy compared to established elements such as Allman and Frey (Ibrahimbegović and Frey, 1992). While MLH8N slightly overestimates the deflection on the coarsest mesh, it quickly approaches the reference solutions with mesh refinement, indicating robust numerical stability. Its consistent performance across all mesh levels, especially its accuracy on finer meshes, highlights MLH8N as a reliable and efficient element suitable for membrane-dominated problems.

3.1.2 Square Plate with Two Adjacent Edges Unconstrained and the Remaining Edges Fixed

A square plate with dimensions L = 10, h = 0.4, and E = 3600, featuring two neighboring free edges and two fixed edges, is evaluated to test the efficacy of the suggested finite element model. This study, previously examined by other researchers (Abderrahmani et al., 2016; Belarbi and Charif, 1999; Belounar and Guenfoud, 2005; De Rosa and Franciosi, 1990), evaluates two loading scenarios: a concentrated force P = 100 applied at the free corner A and a uniformly distributed load q=0.9, with the corresponding results detailed in **Tables 4** and **5**.

Case 1: Plate Under Concentrated Load (ν=0.0)

Table 4 Square Plate with Two Adjacent Edges Unconstrained and the Remaining Edges Fixed, exposed to a concentrated load

Mesh	Normalized Maximum Deflection				
	R4 (Belounar and Guenfoud, 2005)	SBH8 (Belarbi and Charif, 1999)	SBRP (Belounar and Guenfoud, 2005)	SBRPK (Abderrahmani et al., 2016)	**MLH8N**
2x2	5.220	24.515	24.247	122.28	**24.5051**
4x4	19.547	99.631	99.374	124.75	**99.6262**
6x6	36.679	119.52	119.424	-	**119.5254**
8x8	52.778	124.37	124.323	125.30	**124.3939**
9x9	59.918	125.41	125.368	125.37	**125.4344**
Reference solution (De Rosa and Franciosi, 1990)	**125.52**				

Case 2: Plate subjected to distributed load

Table 5 Square plate with two adjacent edges free and the others clamped subjected to distributed load (ν=0.3)

Mesh	Normalized deflection (max)				
	R4 (Belounar and Guenfoud, 2005)	SBH8(Belarbi and Charif, 1999)	SBRP (Belounar and Guenfoud, 2005)	SBRPK (Abderrahmani et al., 2016)	**MLH8N**
2x2	0.951	3.775	3.735	16.23	**3.7739**
4x4	3.039	14.850	14.811	18.03	**14.8499**
6x6	5.534	17.858	17.845	-	**17.8575**
8x8	7.887	18.489	18.483	18.51	**18.4889**
9x9	8.935	18.571	18.604	18.54	**18.6086**
Analytic sol. (De Rosa and Franciosi, 1990)	**18.64**				

The accuracy and convergence behavior of the MLH8N element are evaluated through the static analysis of a square plate with two adjacent edges fixed and the remaining edges free, subjected to both concentrated and uniformly distributed loads (Tables 4 and 5). For both loading scenarios, the proposed element demonstrates a superior convergence rate compared to the displacement-based R4 element, which exhibits severe locking. Under a concentrated load, the MLH8N element achieves a normalized deflection of 125.4344, closely matching the analytical reference of 125.52. Similarly, under a distributed load, the element provides a high-precision result of 18.6086, diverging by only 0.17% from the benchmark solution. These results are in excellent agreement with established strain-based formulations such as SBH8 and SBRP, confirming the robustness of the MLH8N element in eliminating shear locking and its reliability for the analysis of isotropic structures under various load configurations.

3.1.3 Static analysis of functionally graded (FGM) square plates under uniform and sinusoidal loads

Let us consider an Al/ZrO$_2$ square plate subjected to a uniform transverse load q_0, as illustrated in **Figure 4 (a)** and **(b)**, with clamped (CCCC) and simply supported (SSSS) boundary conditions, and for different values of the gradient index (n = 0, 0.5, 1, 2). The non-dimensional central deflection is evaluated using the following expression: $W = (100 w_c E_m h^3/12\ q_0\, a^4\, (1-\nu^2))$. The results obtained with the proposed MLH8N element are presented in **Table 6** and in **Figures 5** and **6** for a thickness-to-side ratio of a/h = 5. These results are compared with those obtained using the SBQP20 element and with other reference solutions available in the literature, including IGA-Quadratic, MITC4, ES-DSG3, NS-DSG3, kip-Ritz, and MLPG. The comparison demonstrates the accuracy and fast convergence of the MLH8N element for both boundary conditions.

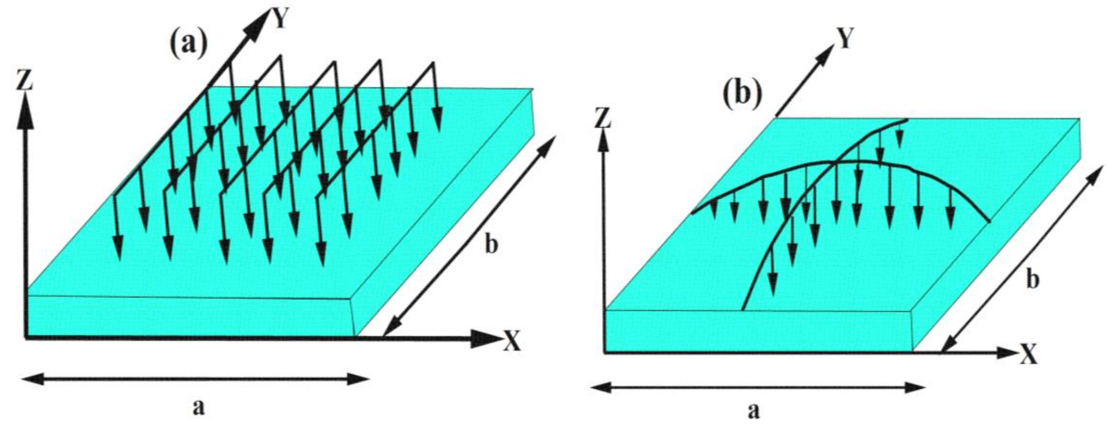

Figure 4 Square FG plates under uniform load **(a)** and sinusoidal load **(b)**

Table 6 Dimensionless deflection (W) of Al/ZrO_2 square plates under uniform loads with (a/h = 5)

Boundary condition	Methods	*n*			
		0	0.5	1	2
CCCC	SBQP20 (8 × 8) (Belounar et al., 2022)	0.0750	0.0999	0.1165	0.1349
	MLH8N (8 × 8)	**0.0736**	**0.0978**	**0.1141**	**0.1324**
	SBQP20 (12x12) (Belounar et al., 2022)	0.0756	0.1007	0.1175	0.1360
	MLH8N (12 × 12)	**0.0755**	**0.1004**	**0.1172**	**0.1358**
	SBQP20 (16x16) (Belounar et al., 2022)	0.0758	0.1010	0.1178	0.1364
	MLH8N (16 × 16)	**0.0762**	**0.1013**	**0.1183**	**0.1371**
	SBQP20 (20x20) (Belounar et al., 2022)	0.0759	0.1011	0.1180	0.1366
	MLH8N (20 × 20)	**0.0765**	**0.1017**	**0.1188**	**0.1376**
	SBQP20 (32x32) (Belounar et al., 2022)	0.0760	0.1012	0.1182	0.1368
	MLH8N (32 × 32)	**0.0768**	**0.1022**	**0.1194**	**0.1382**
	IGA-Quadratic (Valizadeh et al., 2013)	0.0760	0.1013	0.1183	0.1369
	MITC4 (Nguyen-Xuan et al., 2012)	0.0758	0.1010	0.1179	0.1365
	ES-DSG3 (Nguyen-Xuan et al., 2012)	0.0761	0.1013	0.1183	0.1370
	NS-DSG3(32x32) (Nguyen-Xuan et al., 2012)	0.0764	0.1018	0.1189	0.1376
	kip-Ritz (Lee et al., 2009)	0.0774	0.1034	0.1207	0.1404
	MLPG (Gilhooley et al., 2007)	0.0731	0.1073	0.1253	0.1444
SSSS	SBQP20 (8 × 8) (Belounar et al., 2022)	0.1703	0.2305	0.2696	0.3088
	MLH8N (8 × 8)	**0.1654**	**0.2235**	**0.2617**	**0.3000**
	SBQP20 (12x12) (Belounar et al., 2022)	0.1711	0.2316	0.2709	0.3103
	MLH8N (12 × 12)	**0.1695**	**0.2291**	**0.2682**	**0.3074**
	SBQP20 (16x16) (Belounar et al., 2022)	0.1713	0.2320	0.2714	0.3109
	MLH8N (16 × 16)	**0.1709**	**0.2311**	**0.2705**	**0.3100**
	SBQP20 (20x20) (Belounar et al., 2022)	0.1714	0.2321	0.2716	0.3111
	MLH8N (20 × 20)	**0.1715**	**0.2320**	**0.2715**	**0.3112**
	SBQP20 (32x32) (Belounar et al., 2022)	0.1716	0.2323	0.2718	0.3114

MLH8N (32 × 32)	**0.1722**	**0.2329**	**0.2727**	**0.3125**
IGA-Quadratic (Valizadeh et al., 2013)	0.1717	0.2324	0.2719	0.3115
MITC4(Nguyen-Xuan et al., 2012)	0.1715	0.2317	0.2704	0.3093
ES-DSG3 (Nguyen-Xuan et al., 2012)	0.1700	0.2296	0.2680	0.3066
NS-DSG3(32x32) (Nguyen-Xuan et al., 2012)	0.1717	0.2321	0.2709	0.3099
kip-Ritz (Lee et al., 2009)	0.1722	0.2403	0.2811	0.3221
MLPG (Gilhooley et al., 2007)	0.1671	0.2505	0.2905	0.328

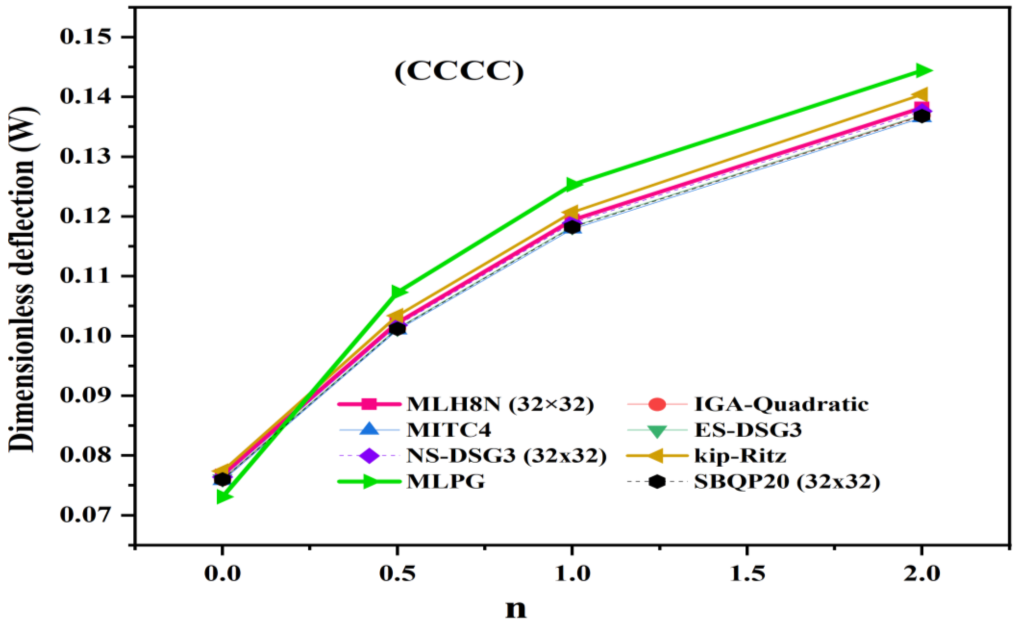

Figure 5 Dimensionless deflection (W) of square (Al/ZrO₂) plates under uniform load with clamped edges (CCCC)

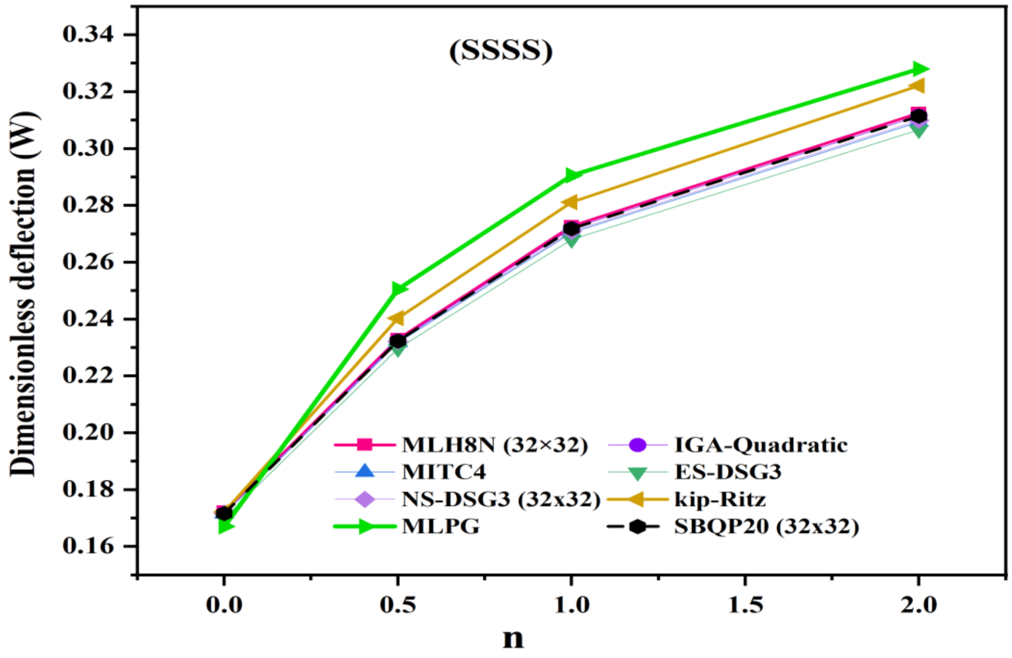

Figure 6 Dimensionless deflection (W) of square (Al/ZrO₂) plates under uniform load with simply supported edges (SSSS)

Table 6 shows that the proposed MLH8N element yields highly accurate results for Al/ZrO$_2$ square plates subjected to uniform loads under both CCCC and SSSS boundary conditions. Across all mesh densities (8×8 to 32×32) and material gradient indices (n = 0 to 2), MLH8N results closely match benchmark solutions such as IGA-Quadratic, MITC4, and ES-DSG3, and consistently outperform alternative methods like NS-DSG3, kip-Ritz, MLPG, and even SBQP20 in terms of accuracy and convergence. Notably, MLH8N exhibits remarkable numerical stability and precision even with coarse meshes, confirming its robustness and computational efficiency. These attributes make MLH8N a highly reliable tool for the simulation of functionally graded material (FGM) plates, particularly in demanding scenarios.

3.2 Free vibration validation

3.2.1 Out-of-plane bending vibrations of a rectangular isotropic elastic beam

This example examines the out-of-plane bending vibrations of the isotropic elastic beam depicted in **Figure 7**. Analytical equations for the transverse natural frequencies are available, as exemplified in (Den Hartog, 1985), and are articulated as follows:

$$fn = \frac{a_{\mathrm{n}}}{2\pi}\sqrt{\frac{EI}{\varphi S L^4}}\,; \qquad I = \frac{bh^3}{12}; \quad S = b\ x\ h \tag{17}$$

where EI represents the bending stiffness of the section, φ denotes the mass density of the beam material, and a_{n} is a numerical constant that varies for each mode. Figure 7 illustrates the isotropic elastic beam, which is represented by a uniform mesh with 10 elements along the length, one element along the breadth, and one element throughout the thickness. **Table 7** summarizes the first three numerical natural frequencies together with the relative errors compared to the analytical values for three configurations. Clamped-Free (CF), Clamped-Clamped (CC) and Simply Supported (SS).

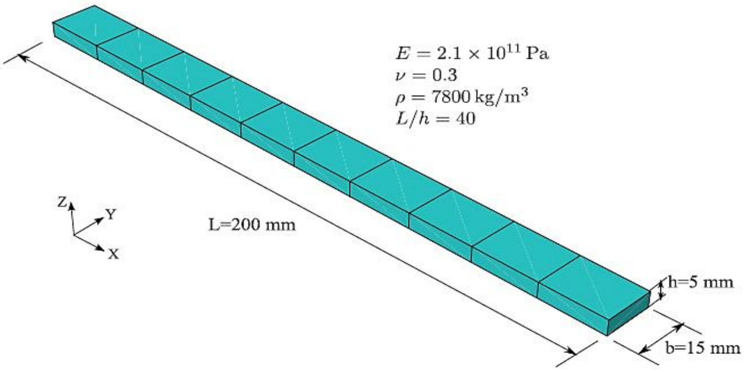

Figure 7 The isotropic elastic beam is modelled using ten hexahedral elements with dimensions of 10×1×1

Table 7 First three natural frequencies of out-of-plane bending for the isotropic elastic beam

(Total DOFs)	C3D8 (Zouari et al., 2015)	C3D8I (Zouari et al., 2015)	C3D20 (Zouari et al., 2015)	SFR8 (Zouari et al., 2015)	SFR8I (Zouari et al., 2015)	**MLH8N (10x1)**	**MLH8N (22x22)**	Analytical Equation (Zouari et al., 2015)
C-F								
f$_1$ (Hz)	268.85	105.44	106.46	111.23	105.54	**105.39**	**105.1497**	104.892
f$_2$ (Hz)	1,661.1	658.46	669.49	703.04	667.26	**671.394**	**660.158**	655.578
f$_3$ (Hz)	4,583.2	1,853.2	1,888.4	2,000.4	1,897.8	**1,940.514**	**1,857.805**	1,838.599
C-C								
f$_1$ (Hz)	1,715.2	690.39	691.94	725.65	685.45	**689.197**	**673.165**	655.578
f$_2$ (Hz)	4,704.5	1,943.7	1,924.9	2,042.0	1,929.3	**1,974.105**	**1,865.473**	1,838.599
f$_3$ (Hz)	9,149.1	3,929.1	3,825.4	4,123.9	3,894.5	**4,083.602**	**3,688.409**	3,605.680

S-S								
f_1 (Hz)	757.56	295.24	294.65	309.16	294.85	**296.6144**	**294.517**	294.104
f_2 (Hz)	3,019.5	1,194.8	1,185.2	1,246.8	1,188.3	**1,217.858**	**1,184.123**	1,176.417
f_3 (Hz)	6,751.7	2,741.8	2,692.6	2,842.3	2,706.5	**2,858.447**	**2,686.960**	2,646.940

Table 7 presents the first three natural frequencies for an isotropic elastic beam in out-of-plane bending under various boundary conditions, comparing results from the proposed MLH8N element against established solid and shell elements, all computed using a 10×1 mesh (Zouari et al., 2015), as well as the analytical solution (Zouari et al., 2015). Across all boundary conditions cantilever-free (C-F), clamped-clamped (C-C), and simply supported (S-S) the MLH8N element demonstrates excellent agreement with analytical frequencies, especially when refined to a 22×22 mesh, yielding deviations typically below 2% from exact values. Notably, even with a coarse mesh (10×1), MLH8N outperforms or matches the accuracy of solid elements like C3D8 and C3D8I, which tend to significantly overpredict the natural frequencies (e.g., f_1 under C-F is 268.85 Hz for C3D8 versus 105.39 Hz for MLH8N, close to the analytical 104.892 Hz). Compared to higher-order solid elements like C3D20 and specialized shell elements like SFR8 and SFR8I, MLH8N delivers competitive results but with the advantage of a lower computational cost and fewer degrees of freedom required to achieve similar accuracy. Particularly under clamped-clamped conditions, MLH8N's frequencies (e.g., f_3 = 4,083.602 Hz with a 10×1 mesh) remain closer to the analytical value (3,605.680 Hz) than those from C3D8 (9,149.1 Hz) or SFR8 (4,123.9 Hz), highlighting its superior convergence behavior and reduced stiffness overestimation often observed in traditional solid elements. These results underscore the MLH8N element's capability to combine high accuracy with computational efficiency, making it especially advantageous for dynamic analyses of slender beams and structures where both precision and resource optimization are essential.

3.2.2 Transverse vibrations of a thick square plate

This subsection examines the transverse free vibrations of a thick square plate with a side length of 10 m and a slenderness ratio of 10 (**Figure 8**). Two boundary conditions will be examined: first, the square plate is entirely clamped (CCCC), and second, the plate is clamped on one side (X = 0), simply supported at two ends (Y = 0 and X = a), and free on the remaining side (CSSF). Liew et al. (1993) computed the transverse natural frequencies of this square plate using the Pb2-Ritz method. The square plate is represented by a regular mesh with 8×8×1 components, as illustrated in Figure 8. **Table 8** encapsulates the findings of the initial four transverse natural frequencies along with the corresponding relative errors compared to the reference values presented in (Liew et al., 1993)

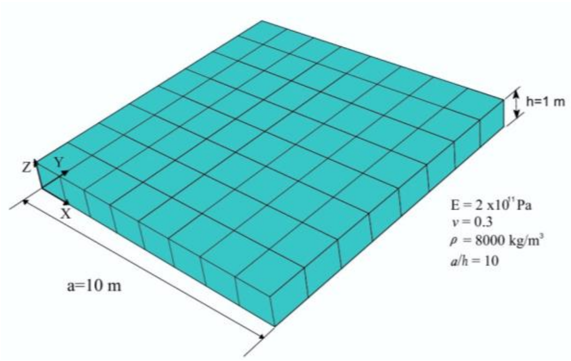

Figure 8 Thick square plate modeled using an 8×8×1 mesh of hexahedral elements

Table 8 First four transverse natural frequencies (Hz) of the thick square plate

(Total DOFs)	C3D8 (Zouari et al., 2015)	C3D8I (Zouari et al., 2015)	C3D20 (Zouari et al., 2015)	SFR8 (Zouari et al., 2015)	SFR8I (Zouari et al., 2015)	**MLH8N (8x8)**	**MLH8N (22x22)**	Pb2-Ritz method (Liew et al., 1993)
CCCC								
$f_1 = f_{11}$	75.385	78.636	81.431	88.894	81.764	**83.993**	**79.010**	**78.322**
$f_{12} = f_{21}$	145.25	150.11	156.46	172.77	160.56	**169.679**	**151.817**	**149.396**
$f_4 = f_{22}$	187.73	199.97	219.53	241.53	225.76	**249.349**	**214.047**	**209.384**

CSSF								
$f_1 = f_{11}$	38.095	38.539	38.933	41.650	38.947	**39.3501**	**38.203**	**38.491**
$f_2 = f_{12}$	61.311	65.884	69.098	74.282	68.967	**71.95814**	**68.260**	**69.317**
$f_3 = f_{21}$	112.07	112.09	113.79	124.09	116.11	**119.3134**	**110.895**	**110.783**
$f_4 = f_{13}$	120.5	126.41	138.08	151.07	139.29	**128.044**	**136.531**	**137.077**

Table 8 presents the first four transverse natural frequencies of a substantial square plate under fully clamped (CCCC) and clamped–simply supported–free (CSSF) boundary conditions, comparing the proposed MLH8N element to established solid and shell elements, as well as to the Pb2-Ritz method serving as the reference solution. All comparative analyses, including those from C3D8, C3D8I, C3D20, SFR8, SFR8I, and the Pb2-Ritz method, were performed using an identical 8×8 mesh for consistency. A detailed comparison reveals that while the SFR8 element provides reasonable estimates, it consistently overestimates the natural frequencies, particularly for higher modes and under both CCCC and CSSF conditions (for example, under CCCC, SFR8 predicts f_{11} = 88.894 Hz and f_{22} = 241.53 Hz, both notably above the reference values of 78.322 Hz and 209.384 Hz, respectively). In contrast, the MLH8N element, especially when refined to a 22×22 mesh, yields results much closer to the reference (f_{11} = 79.010 Hz, f_{22} = 214.047 Hz), demonstrating superior accuracy and convergence. Even with the same coarse 8×8 mesh, MLH8N produces results consistently closer to the analytical benchmark than lower-order solid elements like C3D8, which tends to underestimate the lower frequencies. Under CSSF conditions, MLH8N maintains strong accuracy, particularly in higher modes where conventional elements often show larger discrepancies; for instance, the fourth mode f_{13} is computed as 128.044 Hz (MLH8N, 8×8 mesh) and 136.531 Hz (MLH8N, 22×22 mesh), compared to 137.077 Hz for the reference, while SFR8 significantly overestimates this value (f_{13} = 151.07 Hz). These findings clearly highlight the robustness and reliability of MLH8N, which not only avoids the overestimation observed with SFR8 but also achieves high fidelity across all modes, requiring fewer degrees of freedom and avoiding numerical issues such as shear locking. This balance of computational efficiency and high accuracy makes the MLH8N element highly effective for modeling plates with mixed boundary conditions and for applications where vibration analysis demands reliable predictive performance.

3.2.3 Free Vibration of Square Plates

This section investigates the free vibration behavior of a square plate, to evaluate the influence of different boundary conditions using the present numerical method. Convergence studies are performed for both simply supported and fully clamped edge conditions. The results are expressed in terms of the non-dimensional frequency parameter: $\lambda = ((\omega^2 \times \rho \times h \times L^4)/D)^{1/4}$ and are summarized in **Tables 9** and **10** for the fully simply supported (SSSS) and fully clamped (CCCC) cases. The study considers plates with side lengths a = b =L= 10.00 m and thicknesses h = 0.05m (thin plate) and h = 1 m (thick plate), made of a material characterized by a young's modulus $E = 200 \times 10^9$ N/m², Poisson's ratio ν = 0.3, shear correction factor k = 0.8333, and mass density ρ = 8000 kg/m³. A regular 22 x 22 mesh grid is employed for the computations.

In addition, **Table 11** presents the non-dimensional frequencies for square plates with other boundary conditions, such as (SSSF, SFSF, CCCF, CFCF, and CFSF), using the same geometric and material parameters (a, b, ν, k, E, and ρ) and the same mesh grid of 22 x 22 elements, except that the non-dimensional frequency parameter is defined as: $(\lambda = (\omega L^2(\rho h/D)^{1/2})$.

Table 9 Non-dimensional frequency parameter λ of a SSSS plate

h/a	Mode	Method							
		DSG3 (Nguyen-Thoi et al., 2012)	ES-DSG3 (Nguyen-Thoi et al., 2012)	CS-DSG3 (Nguyen-Thoi et al., 2012)	MIN3 (Nguyen-Thoi et al., 2012)	MITC4 (M) (Nguyen-Thoi et al., 2012)	MITC4 (Nguyen-Thoi et al., 2012)	**MLH8N**	Exact (Abbassian et al., 1987)
0.005	1	4.4781	4.4537	4.4440	4.4600	4.4464	4.4477	**4.454**	4.4430
	2	7.0905	7.0565	7.0276	7.0732	7.0479	7.0531	**7.070**	7.0250
	3	7.1718	7.0729	7.0306	7.1003	7.0479	7.0531	**7.070**	7.0250
	4	9.1455	8.9731	8.8949	9.0220	8.9142	8.9247	**8.983**	8.8860
	5	10.1643	10.0410	9.94620	10.0972	10.0200	10.0349	**10.066**	9.93500
	6	10.1814	10.0422	9.94630	10.0997	10.0200	10.0349	**10.067**	9.93500
0.1	1	4.3809	4.3759	4.3674	4.4178	4.3694	4.3711	**4.307**	4.3700

	2	6.7854	6.7692	6.7456	6.9231	6.7618	6.7692	**6.678**	6.7400
	3	6.8037	6.7834	6.7478	6.9373	6.7618	6.7692	**6.678**	6.7400
	4	8.4543	8.4173	8.3587	8.7030	8.3757	8.3872	**8.251**	8.3500
	5	9.3441	9.2968	9.2238	9.6856	9.2800	9.3009	**9.173**	9.2200
	6	9.3457	9.2976	9.2238	9.6866	9.2800	9.3009	**9.187**	9.2200

Table 10 Non-dimensional frequency parameter λ of a CCCC plate

h/a	Mode	Method							
		DSG3 (Nguyen -Thoi et al., 2012)	ES-DSG3 (Nguyen-Thoi et al., 2012)	CS-DSG3 (Nguyen-Thoi et al., 2012)	MIN3 (Nguyen-Thoi et al., 2012)	MITC4 (M) (Nguyen-Thoi et al., 2012)	MITC4 (Nguyen-Thoi et al., 2012)	**MLH8N**	Exact (Abbassian et al., 1987)
0.005	1	6.0889	6.0158	6.0043	6.0417	6.0073	6.0140	**6.059**	5.9990
	2	8.7239	8.6075	8.576	8.6621	8.6083	8.6252	**8.714**	8.568
	3	8.8202	8.6353	8.5848	8.703	8.6083	8.6252	**8.714**	8.568
	4	10.8567	10.5252	10.4260	10.6330	10.4466	10.4750	**10.724**	10.4070
	5	11.8519	11.6032	11.4990	11.7280	11.6016	11.6390	**11.772**	11.4720
	6	11.8845	11.6293	11.5258	11.7541	11.6298	11.6661	**11.779**	11.4980
0.1	1	5.7337	5.7141	5.7077	5.9011	5.7118	5.7166	**5.73**	5.7100
	2	7.9381	7.8990	7.8810	8.314	7.9102	7.9204	**7.94**	7.8800
	3	7.9686	7.9206	7.8873	8.3403	7.9102	7.9204	**7.94**	7.8800
	4	9.4589	9.3896	9.3357	10.011	9.3618	9.3764	**9.43**	9.3300
	5	10.2760	10.1935	10.1273	10.9780	10.2099	10.2280	**10.25**	10.1300
	6	10.3246	10.2411	10.1754	11.0164	10.2590	10.2771	**10.30**	10.1800

Tables 9 and 10 present the non-dimensional frequency parameter λ for square plates with simply supported (SSSS) and fully clamped (CCCC) boundary conditions, respectively, across various thickness ratios (h/a) and vibration modes. The performance of the proposed MLH8N element is compared against several established finite element formulations including DSG3, ES-DSG3, CS-DSG3, MIN3, MITC4(M), and MITC4 as well as exact solutions from classical plate theory. Across both thin (h/a = 0.005) and moderately thick (h/a = 0.1) plate scenarios, MLH8N consistently exhibits excellent agreement with exact solutions, with deviations typically within a few percent for all modes. For instance, under SSSS conditions at h/a = 0.005, MLH8N predicts the fundamental frequency parameter as 4.454, closely matching the exact value of 4.443, and maintains similarly close accuracy for higher modes. Under CCCC conditions at the same thickness ratio, MLH8N predicts λ_1 = 6.059, nearly identical to the exact 5.999, reflecting a deviation below 1%. While other elements such as MITC4 and CS-DSG3 also demonstrate good accuracy, MLH8N often surpasses them, especially in higher vibration modes where traditional elements tend to exhibit larger discrepancies due to shear locking and membrane-bending coupling effects. Moreover, MLH8N maintains robust and reliable performance for thicker plates (h/a = 0.1), where many lower-order elements begin to show more significant deviations from exact values. These results underscore the MLH8N element's high precision, efficient convergence, and reduced sensitivity to mesh distortion and locking phenomena, establishing it as a highly reliable and computationally efficient choice for dynamic analyses of plates across a wide range of thicknesses and boundary conditions.

Table 11 Non-dimensional natural frequencies λ of a thin square plate (h/a = 0.005) discretized by a uniform mesh of 22 × 22 elements under various boundary conditions, where $\lambda = (\omega a^2 (\rho h/D)^{1/2})$

		Mode sequence number			
Plate type	Methods	1	2	3	4
SSSF	**MLH8N**	**11.70492**	**27.90186**	**41.56647**	**59.8848**
	DSG3(Nguyen-Thoi et al., 2012)	11.7553	28.258	41.8252	61.1274
	MIN3 (Nguyen-Thoi et al., 2012)	11.7305	28.021	41.7375	60.3199
	ES-DSG3 (Nguyen-Thoi et al., 2012)	11.6817	27.8143	41.3866	59.5521
	MITC4 (Nguyen-Thoi et al., 2012)	11.7085	27.8259	41.5907	59.4952

	CS-DSG3 (Nguyen-Thoi et al., 2012)	11.7117	27.9075	41.6054	59.8642
	Exact (Leissa, 1969)	**11.6850**	**27.7560**	**41.1970**	**59.0660**
SFSF	**MLH8N**	**9.6467**	**16.1596**	**36.9332**	**39.2728**
	DSG3 (Nguyen-Thoi et al., 2012)	9.6608	16.3096	37.5011	39.4050
	MIN3 (Nguyen-Thoi et al., 2012)	9.6591	16.2185	37.1384	39.4010
	ES-DSG3 (Nguyen-Thoi et al., 2012)	9.6402	16.1214	36.8606	39.1664
	MITC4 (Nguyen-Thoi et al., 2012)	9.6560	16.1594	36.8250	39.3439
	CS-DSG3 (Nguyen-Thoi et al., 2012)	9.6523	16.1663	36.9537	39.3145
	Exact (Leissa, 1969)	**9.6310**	**16.1350**	**36.7260**	**38.9450**
CCCF	**MLH8N**	**24.1422**	**40.9051**	**64.4438**	**79.1750**
	DSG3 (Nguyen-Thoi et al., 2012)	24.2149	41.4350	64.6795	80.2128
	MIN3 (Nguyen-Thoi et al., 2012)	24.1257	40.6903	64.4940	78.8210
	ES-DSG3 (Nguyen-Thoi et al., 2012)	23.8927	40.1428	63.4463	77.6415
	MITC4 (Nguyen-Thoi et al., 2012)	24.0559	40.1776	64.2683	77.5923
	CS-DSG3 (Nguyen-Thoi et al., 2012)	24.0220	40.3201	64.0603	77.9933
	Exact (Leissa, 1969)	**24.0200**	**40.0390**	**63.4930**	**76.7610**
CFCF	**MLH8N**	**22.3002**	**26.7678**	**44.6314**	**62.1495**
	DSG3 (Nguyen-Thoi et al., 2012)	22.3132	27.0330	45.4552	62.2851
	MIN3 (Nguyen-Thoi et al., 2012)	22.3122	26.7138	44.4375	62.2847
	ES-DSG3 (Nguyen-Thoi et al., 2012)	22.1684	26.4128	43.8441	61.4711
	MITC4 (Nguyen-Thoi et al., 2012)	22.3107	26.5333	43.7558	62.2403
	CS-DSG3 (Nguyen-Thoi et al., 2012)	22.2521	26.5322	43.9719	61.9548
	Exact (Leissa, 1969)	**22.2720**	**26.5290**	**43.6640**	**64.4660**
CFSF	**MLH8N**	**15.2485**	**20.7296**	**40.2598**	**50.0389**
	DSG3 (Nguyen-Thoi et al., 2012)	15.2635	20.9362	40.9260	50.1777
	MIN3 (Nguyen-Thoi et al., 2012)	15.2635	20.7563	40.3242	50.1788
	ES-DSG3 (Nguyen-Thoi et al., 2012)	15.2002	20.5789	39.9116	49.7129
	MITC4 (Nguyen-Thoi et al., 2012)	15.2590	20.6440	39.8569	50.1204
	CS-DSG3 (Nguyen-Thoi et al., 2012)	15.2385	20.6539	40.0256	49.9966
	Exact (Leissa, 1969)	**15.2850**	**20.6730**	**39.8820**	**49.5000**

Table 11 reports the non-dimensional natural frequencies λ of a thin square plate (h/a = 0.005) discretized with a 22 × 22 mesh under various mixed boundary conditions, comparing the results obtained from the proposed MLH8N element with several established finite element formulations including DSG3, ES-DSG3, CS-DSG3, MIN3, and MITC4 as well as exact solutions. Across all boundary conditions examined, the MLH8N element demonstrates excellent agreement with exact results, with deviations typically within a few tenths of a percent to about 1%, confirming its high accuracy and robust predictive capability. For example, under the SSSF condition, the MLH8N prediction for the fundamental frequency is 11.70492, differing by less than 0.2% from the exact value of 11.6850, and similar close agreement persists across higher modes. Likewise, under the CCCF boundary condition, MLH8N computes the first mode as 24.1422, closely matching the exact 24.0200, indicating a deviation below 0.5%. While other elements such as MITC4 and CS-DSG3 also yield accurate results, the MLH8N element frequently surpasses them in matching the exact solutions, particularly in higher modes where conventional elements sometimes show greater discrepancies due to numerical errors or membrane-bending coupling effects. Furthermore, MLH8N consistently performs well across boundary cases involving combinations of clamped, simply supported, and free edges, which often pose challenges for standard shell elements. These results highlight the MLH8N element's superior accuracy, excellent convergence behavior, and reduced sensitivity to complex boundary conditions, establishing it as a highly reliable and computationally efficient option for dynamic analysis of thin plate structures.

3.2.4 Free Vibration Analysis of Simply Supported Functionally Graded Material (FGM) Square Plates

Convergence tests are performed on fully simply supported Al/Al_2O_3 square plates with three thickness ratios (a/h = 5, 10, 20) and various values of the volume fraction exponent (n = 0, 0.5, 1, 4, 10) to evaluate the stability of the proposed element. Reference solutions include SBQP20, ES-DSG, MITC4, DSG3, kip-Ritz, and HSDT. The fundamental non-dimensional frequency is defined as: $\varpi = \omega h(\sqrt{\rho_c/E_c})$. The results obtained using the MLH8N element with mesh sizes of 8×8, 12×12, 16×16, and 20×20 are presented in **Table 12** for validation and comparison.

Table 12 Dimensionless fundamental frequency (ϖ) of SSSS Al/Al_2O_3 square plate

a/h	Element	*n*				
		0	0.5	1	4	10
5	**MLH8N(8×8)**	**0.21858**	**0.18692**	**0.16883**	**0.14438**	**0.13667**
	MLH8N(12×12)	**0.2144**	**0.1833**	**0.16555**	**0.14164**	**0.13413**
	MLH8N(16×16)	**0.21297**	**0.18206**	**0.16442**	**0.1407**	**0.13326**
	MLH8N(20×20)	**0.21231**	**0.18149**	**0.16391**	**0.14027**	**0.13286**
	SBQP20 (8×8) (Belounar et al., 2022)	0.21055	0.17991	0.16262	0.13932	0.13198
	SBQP20 (12×12) (Belounar et al., 2022)	0.21091	0.18020	0.16284	0.13946	0.13214
	SBQP20 (16×16) (Belounar et al., 2022)	0.21104	0.18030	0.16292	0.13951	0.13219
	SBQP20 (20×20) (Belounar et al., 2022)	0.21110	0.18035	0.16296	0.13953	0.13222
	ES-DSG (20×20) (Nguyen-Xuan et al., 2011)	0.21218	0.18114	0.16351	0.13992	0.13272
	DSG3 (16×16) (Nguyen-Xuan et al., 2011)	0.21335	0.18216	0.16444	0.14069	0.13343
	MITC4 (16×16) (Nguyen-Xuan et al., 2011)	0.21182	0.18082	0.16323	0.13968	0.13251
	HSDT (Belounar et al., 2022)	0.21210	0.18190	0.16400	0.13830	0.13060
	kip-Ritz (Zhao et al., 2009)	0.2055	0.1757	0.1587	0.1356	0.1284
	Reference (Hosseini-Hashemi et al., 2011)	0.2112	0.1805	0.1631	0.1397	0.1324
10	**MLH8N(8×8)**	**0.06003**	**0.05101**	**0.04598**	**0.03974**	**0.03799**
	MLH8N(12×12)	**0.05870**	**0.04987**	**0.04495**	**0.03886**	**0.03716**
	MLH8N(16×16)	**0.05825**	**0.04949**	**0.04461**	**0.03857**	**0.03687**
	MLH8N(20×20)	**0.05804**	**0.04931**	**0.04445**	**0.03843**	**0.03674**
	SBQP20 (8×8) (Belounar et al., 2022)	0.05744	0.04878	0.04401	0.03809	0.03641
	SBQP20 (12×12) (Belounar et al., 2022)	0.05758	0.04889	0.04410	0.03815	0.03649
	SBQP20 (16×16) (Belounar et al., 2022)	0.05763	0.04893	0.04413	0.03818	0.03652
	SBQP20 (20×20) (Belounar et al., 2022)	0.05765	0.04895	0.04415	0.03819	0.03653

	ES-DSG (20×20) (Nguyen-Xuan et al., 2011)	0.05800	0.04924	0.04439	0.03839	0.03673
	DSG3 (16×16) (Nguyen-Xuan et al., 2011)	0.05834	0.04954	0.04467	0.03861	0.03693
	MITC4 (16×16) (Nguyen-Xuan et al., 2011)	0.05787	0.04913	0.04429	0.03830	0.03665
	HSDT (Belounar et al., 2022)	0.05777	0.04917	0.04426	0.03811	0.03642
	kip-Ritz (Zhao et al., 2009)	0.05673	0.04818	0.04346	0.03757	0.03591
	Reference (Hosseini-Hashemi et al., 2011)	0.0577	0.0490	0.0442	0.0382	0.0366
20	**MLH8N(8×8)**	**0.01543**	**0.01309**	**0.01179**	**0.01023**	**0.00981**
	MLH8N(12×12)	**0.01507**	**0.01278**	**0.01151**	**0.00999**	**0.00958**
	MLH8N(16×16)	**0.01495**	**0.01268**	**0.01142**	**0.00991**	**0.00950**
	MLH8N(20×20)	**0.01489**	**0.01263**	**0.01138**	**0.00987**	**0.00946**
	SBQP20 (8×8) (Belounar et al., 2022)	0.01473	0.01248	0.01126	0.00977	0.00937
	SBQP20 (12×12) (Belounar et al., 2022)	0.01477	0.01251	0.01128	0.00979	0.00939
	SBQP20 (16×16) (Belounar et al., 2022)	0.01478	0.01253	0.01129	0.00980	0.00940
	SBQP20 (20×20) (Belounar et al., 2022)	0.01479	0.01253	0.01129	0.00980	0.00941
	ES-DSG (20×20) (Nguyen-Xuan et al., 2011)	0.01488	0.01261	0.01137	0.00986	0.00946
	DSG3 (16×16) (Nguyen-Xuan et al., 2011)	0.01498	0.01270	0.01145	0.00993	0.00952
	MITC4 (16×16) (Nguyen-Xuan et al., 2011)	0.01485	0.01258	0.01134	0.00984	0.00944
	kip-Ritz (Zhao et al., 2009)	0.01464	0.01241	0.01118	0.009702	0.009311
	Reference (Hosseini-Hashemi et al., 2011)	0.0148	0.0125	0.0113	0.0098	0.0094

Table 12 presents the dimensionless fundamental frequencies (ϖ) for simply supported (SSSS) Al/Al_2O_3 square plates with various thickness-to-side ratios (a/h = 5, 10, and 20) and volume fraction indices (n = 0, 0.5, 1, 4, and 10). The proposed MLH8N element yields results in very close agreement with the reference values, particularly for finer meshes such as 20×20. Even with coarser meshes (e.g., 8×8 or 12×12), MLH8N demonstrates rapid convergence and excellent accuracy. When compared to other well-established methods including SBQP20, ES-DSG, DSG3, MITC4, HSDT, kip-Ritz, and analytical references, MLH8N exhibits competitive or superior performance. These results confirm the robustness and efficiency of the MLH8N formulation for the dynamic analysis of FGM plates across a broad range of thicknesses and material gradation parameters.

3.2.5 Free Vibration Characteristics of CCCC and SSSS FGM Plates

Tables 13 and **14** present the non-dimensional frequency parameter, defined as $\varpi = \omega a^2/h\sqrt{\rho_c/E_c}$, for square FGM plates composed of SUS304/Si_3N_4. Table 13 reports result for fully clamped (CCCC) boundary conditions, whereas Table 14 provides data for simply supported (SSSS) edges, both considering a side-to-thickness ratio of a/h = 10. The tables list the first five vibration modes for various volume fraction indices ranging from n = 0 (ceramic) to n → ∞ (metal), representing the transition from ceramic-rich to metal-rich properties. The material properties are assumed to vary through the thickness according to a power-law distribution, with Poisson's ratio kept constant.

Table 13 Variation of the frequency parameter ϖ with the volume fraction index n for CCCC square SUS304/Si_3N_4 FGM plates

Boundary condition	Element	Mode	n					
			Ceramic	0.5	1	5	10	Metal
CCCC	Talha and Singh (Talha and Singh, 2010)	1	10.1599	7.0202	6.1489	4.9816	4.7457	4.4410
	MLH8N		**10.1787**	**7.0547**	**6.19085**	**5.04436**	**4.80938**	**4.46526**

	Talha and Singh (Talha and Singh, 2010)	2	19.9367	13.7978	12.0812	9.7440	9.2841	8.7107
	MLH8N		**20.217**	**13.9879**	**12.2618**	**9.95368**	**9.4859**	**8.81856**
	Talha and Singh (Talha and Singh, 2010)	3	19.9367	13.7978	12.0812	9.7440	9.2841	8.7107
	MLH8N		**20.217**	**13.9879**	**12.2618**	**9.95368**	**9.4859**	**8.81856**
	Talha and Singh (Talha and Singh, 2010)	4	28.1367	19.4845	17.0625	13.7350	13.0873	12.2919
	MLH8N		**29.2804**	**20.2291**	**17.7183**	**14.3454**	**13.6672**	**12.7174**
	Talha and Singh (Talha and Singh, 2010)	5	34.6017	23.9945	20.9992	16.8507	16.0556	15.1084
	MLH8N		**35.178**	**24.2843**	**21.2597**	**17.1859**	**16.3711**	**15.2431**

Table 14 Variation of the frequency parameter ϖ with the volume fraction index n for SSSS square SUS304/ Si_3N_4 FGM plates

Boundary condition	Element	Mode	n					
			Ceramic	0.5	1	5	10	Metal
SSSS	Talha and Singh (Talha and Singh, 2010)	1	5.7523	3.9701	3.4845	2.8351	2.6973	2.5154
	MLH8N		**5.65281**	**3.92612**	**3.45102**	**2.82789**	**2.69942**	**2.50705**
	Talha and Singh (Talha and Singh, 2010)	2	14.0336	9.6890	8.4903	6.8941	6.5669	6.1361
	MLH8N		**14.0151**	**9.71907**	**8.53605**	**6.97587**	**6.65677**	**6.18637**
	Talha and Singh (Talha and Singh, 2010)	3	14.0354	9.6906	8.4918	6.8952	6.5680	6.1370
	MLH8N		**14.0151**	**9.71907**	**8.53605**	**6.97587**	**6.65677**	**6.18637**
	Talha and Singh (Talha and Singh, 2010)	4	21.6188	14.9404	13.0959	10.6102	10.1053	9.4515
	MLH8N		**21.9894**	**15.2592**	**13.4022**	**10.9364**	**10.4309**	**9.69662**
	Talha and Singh (Talha and Singh, 2010)	5	27.1449	18.7691	16.4526	13.3057	12.6668	11.8664
	MLH8N		**27.6523**	**19.1508**	**16.8077**	**13.3194**	**12.6543**	**11.9103**

The frequency results presented in Tables 13 and 14 demonstrate the accuracy and efficiency of the proposed MLH8N element for the free vibration analysis of functionally graded square plates made of SUS304/Si_3N_4. For both fully clamped (CCCC) and simply supported (SSSS) boundary conditions, and across all volume fraction indices n, the MLH8N element consistently provides results that are in excellent agreement with the reference values reported by Talha and Singh (2010). The MLH8N values remain very close to the benchmark data for all vibration modes, even at higher material gradation levels. This close correlation confirms the capability of the proposed strain-based hexahedral element to accurately capture the dynamic behavior of FGM plates. Furthermore, the observed consistency highlights the robustness of MLH8N with respect to boundary conditions and material heterogeneity, making it a reliable and efficient tool for vibration analysis of FGM structures.

4 CONCLUSION

In this paper a new multilayer hexahedral 8 nodes membrane and binding rectangular finite element named MLH8N based on the high order of polynomial terms for the three translational displacement field approach is developed for the static and free vibration elastic analysis for isotropic material case which is extended to take into account Functionally Graded Material. This simple element with 24 degrees of freedom in the isotropic and FGM case has shown its efficiency, rapid convergence and excellent agreement towards the analytical solution compared with the available literature results for static and free vibration of thin and thick plates under various boundary conditions and different load type. In this study the results are obtained by using the Gauss numerical integration in 3D. It is worth noting that the current element has proven its superiority over other 2D elements in many cases.

The analysis was limited to isotropic and FGM materials; the effects of material or geometric nonlinearities and the use of other types of composite materials are not addressed here and are the subject of future perspectives.

Author's Contributions: Conceptualization, R. Bourenane, B. Amieur, and S. Abderrahmani; Methodology, R. Bourenane, B. Amieur, and S. Abderrahmani; Software, R. Bourenane; Validation, R. Bourenane, B. Amieur, S. Abderrahmani, and A. M. AL-Nadhari; Formal analysis, R. Bourenane, B. Amieur, and S. Abderrahmani; Investigation, R. Bourenane, B. Amieur, S. Abderrahmani, and A. M. AL-Nadhari; Resources, B. Amieur, S. Abderrahmani, and A. M. AL-Nadhari; Data curation, R. Bourenane; Writing – original draft, R. Bourenane; Writing – review & editing, R. Bourenane, B. Amieur, S. Abderrahmani, and A. M. AL-Nadhari; Visualization, R. Bourenane; Supervision, B. Amieur, S. Abderrahmani, and A. M. AL-Nadhari; Project administration, S. Abderrahmani; Funding acquisition, B. Amieur, S. Abderrahmani, and A. M. AL-Nadhari.

Data Availability: Research data is available in the body of the article.

Editor: Marco L. Bittencourt

References

Abbassian, F., Dawswell, D.J., Knowles, N.C. (1987). Free vibration benchmarks. Atkins Engineering Sciences, Glasgow, UK.

Abderrahmani, S., Maalem, T., Hamadi, D. (2016). On improved thin plate bending rectangular finite element based on the strain approach. International Journal of Engineering Research in Africa 27: 76–86.

Amieur, B., Djermane, M., Hammadi, F. (2017). Nonlinear analysis of degenerated FGM shells. International Journal of Applied Engineering Research 12(21): 11511–11522.

Amieur, B., Djermane, M., Zenkour, A.M., Hammadi, F. (2024). Dynamic buckling analysis of functionally graded shells. Mechanics Based Design of Structures and Machines 52: 4399–4414.

Belarbi, M.T., Charif, A. (1999). Développement d'un nouvel élément hexaédrique simple basé sur le modèle en déformation pour l'étude des plaques minces et épaisses. Revue Européenne des Éléments Finis 8: 135–157.

Belarbi, M.T., Maalem, T. (2005). On improved rectangular finite element for plane linear elasticity analysis. Revue Européenne des Éléments 14: 985–997.

Belounar, A., Boussem, F., Houhou, M.N., Tati, A., Fortas, L. (2022). Strain-based finite element formulation for the analysis of functionally graded plates. Archive of Applied Mechanics 92: 2061–2079.

Belounar, A., Boussem, F., Tati, A. (2023). A novel C0 strain-based finite element for free vibration and buckling analyses of functionally graded plates. Journal of Vibration Engineering and Technologies 11: 281–300.

Belounar, L., Guenfoud, M. (2005). A new rectangular finite element based on the strain approach for plate bending. Thin-Walled Structures 43: 47–63.

Belounar, L., Guerraiche, K. (2014). A new strain based brick element for plate bending. Alexandria Engineering Journal 53: 95–105.

Bouzidi, L., Belounar, L., Guerraiche, K. (2019). Presentation of a new membrane strain-based finite element for static and dynamic analysis. International Journal of Structural Engineering 10: 40–60.

Cetkin, A., Orak, S. (2017). Free vibration analysis of point supported rectangular plates using quadrature element method. Journal of Theoretical and Applied Mechanics 55: 1041–1053.

De Rosa, M.A., Franciosi, C. (1990). Plate bending analysis by the cell method: Numerical comparisons with finite element methods. Computers & Structures 37: 731–735.

Den Hartog, J.P. (1985). Mechanical vibrations. McGraw-Hill.

Derradji, L., Maalem, T., Merzouki, T., Messai, A. (2021). Solid strain based finite element implemented in ABAQUS for static and dynamic plate analysis. Engineering Solid Mechanics 9: 449–460.

Gilhooley, D.F., Batra, R.C., Xiao, J.R., McCarthy, M.A., Gillespie, J.W. (2007). Analysis of thick functionally graded plates by using higher-order shear and normal deformable plate theory and MLPG method with radial basis functions. Composite Structures 80: 539–552.

Guerraiche, K., Belounar, L., Bouzidi, L. (2018). A new eight nodes brick finite element based on the strain approach. Journal of Solid Mechanics 10: 186–199.

Hamadi, D., Maalem, T. (2010). Presentation of an efficient parallelepiped finite element based on the strain approach "SBP8C. Proceedings of the World Congress on Engineering.

Hosseini-Hashemi, S., Fadaee, M., Atashipour, S.R. (2011). A new exact analytical approach for free vibration of Reissner–Mindlin functionally graded rectangular plates. International Journal of Mechanical Sciences 53: 11–22.

Ibrahimbegović, A., Frey, F. (1992). Membrane quadrilateral finite elements with rotational degrees of freedom. Engineering Fracture Mechanics 43: 13–24.

Kareem, M.G., Sadiq, S.E., Al-Raheem, S.K., Alansari, L.S. (2025). Analysis the free vibration of functionally graded material plate by using new displacement function. Results in Engineering 25: 103756.

Lamraoui, L., Benlahmidi, S., Rebiai, C. (2024). Finite element analysis of plates by an accurate strain-based element. Studies in Engineering and Exact Sciences 5: e7569.

Lee, Y.Y., Zhao, X., Liew, K.M. (2009). Thermoelastic analysis of functionally graded plates using the element-free kp-Ritz method. Smart Materials and Structures 18: 035007.

Leissa, A.W. (1969). Vibration of plates. NASA SP-160.

Liew, K.M., Xiang, Y., Kitipornchai, S. (1993). Transverse vibration of thick rectangular plates—I. Comprehensive sets of boundary conditions. Computers & Structures 49: 1–29.

Ma, Y., Zhang, S., Fan, J., Wang, Y., Deng, Z. (2024). Analytical solution of forced vibration of rectangular plates with part through surface crack based on wave propagation method. Computers & Structures 299: 107402.

Messai, A., Belounar, L., Merzouki, T. (2018). Static and free vibration of plates with a strain based brick element. European Journal of Computational Mechanics.

Nguyen-Thoi, T., Phung-Van, P., Nguyen-Xuan, H., Thai-Hoang, C. (2012). A cell-based smoothed discrete shear gap method using triangular elements for static and free vibration analyses of Reissner–Mindlin plates. International Journal for Numerical Methods in Engineering 91: 705–741.

Nguyen-Xuan, H., Tran, L.V., Nguyen-Thoi, T., Vu-Do, H.C. (2011). Analysis of functionally graded plates using an edge-based smoothed finite element method. Composite Structures 93: 3019–3039.

Nguyen-Xuan, H., Tran, L.V., Thai, C.H., Nguyen-Thoi, T. (2012). Analysis of functionally graded plates by an efficient finite element method with node-based strain smoothing. Thin-Walled Structures 54: 1–18.

Pany, C. (2022). An insight on the estimation of wave propagation constants in an orthogonal grid of a simple line-supported periodic plate using a finite element mathematical model. Frontiers in Mechanical Engineering 8.

Pany, C., Parthan, S. (2003). Axial wave propagation in infinitely long periodic curved panels. Journal of Vibration and Acoustics 125: 24–30.

Pany, C., Parthan, S., Mukhopadhyay, M. (2001). Free vibration analysis of an orthogonally supported multi-span curved panel. Journal of Sound and Vibration 241: 315–318.

Pany, C., Rao, G.V. (2002). Calculation of non-linear fundamental frequency of a cantilever beam using non-linear stiffness. Journal of Sound and Vibration 256: 787–790.

Rebiai, C., Saidani, N., Bahloul, E. (2015). A new finite element based on the strain approach for linear and dynamic analysis. Research Journal of Applied Sciences, Engineering and Technology 11.

Ren, S., Shi, H., Liu, Z., Zhang, J., Li, H., Huang, H., Ao, Y. (2022). Finite element analysis and experimental validation of the anterior cruciate ligament and implications for the injury mechanism. Bioengineering 9: 590.

Sabir, A.B., Sfendji, A. (1995). Triangular and rectangular plane elasticity finite elements. Thin-Walled Structures 21: 225–232.

Sheng, W., Zheng, Z., Zhu, H. (2025). A novel approach to palm vein image segmentation combining multi-scale convolution and swin-transformer networks. Scientific Reports 15: 17539.

Słota, E., Wosatko, A. (2025). Comparative analysis of in-plane and out-of-plane bending benchmarks using two finite element packages. Applied Sciences 15.

Talha, M., Singh, B.N. (2010). Static response and free vibration analysis of FGM plates using higher order shear deformation theory. Applied Mathematical Modelling 34: 3991–4011.

Tian, W., Li, H., Zhu, H., Wang, Y., Liu, X., Yang, R., Xie, Y., Zhang, M., Zhu, J., Wang, X. (2024). A review of smart camera sensor placement in construction. Buildings 14: 3930.

Timoshenko, S., Goodier, J.N. (1951). Theory of Elasticity. McGraw-Hill, London.

Valizadeh, N., Natarajan, S., Gonzalez-Estrada, O.A., Rabczuk, T., Bui, T.Q., Bordas, S.P.A. (2013). NURBS-based finite element analysis of functionally graded plates: Static bending, vibration, buckling and flutter. Composite Structures 99: 309–326.

Xing, Y., Li, G., Yuan, Y. (2022). A review of the analytical solution methods for the eigenvalue problems of rectangular plates. International Journal of Mechanical Sciences 221: 107171.

Zhao, X., Lee, Y.Y., Liew, K.M. (2009). Free vibration analysis of functionally graded plates using the element-free kp-Ritz method. Journal of Sound and Vibration 319: 918–939.

Zouari, W., Assarar, M., Meftah, K., Ayad, R. (2015). Free vibration analysis of homogeneous piezoelectric structures using specific hexahedral elements with rotational DOFs. Acta Mechanica 226: 1737–1756.